Scheme I

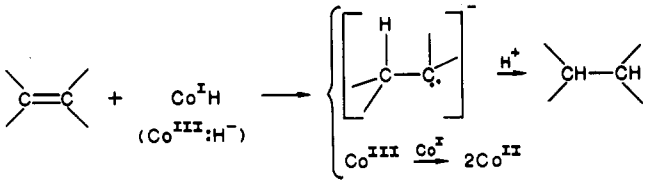

in the rate laws for five of our systems appears to be consistent with such a formulation. Since this path exhibits no kinetic saturation with respect to $[H^+]$ above pH 2, pK_A for the protonation should fall below 0, and the quantity of diprotonated B_{12s} is too small to be detected spectrophotometrically in the solutions at hand. The bimolecular specific rates for reactions of diprotonated B_{12s} with our esters would then exceed 10^4 M^{-1} s^{-1}.

The reduction of the acetylenic ester to fumarate results in a net trans addition, which may be taken to be closely related to the analogous transformation of the parent diacid.[5] The latter was depicted as a heterolytic sequence passing through (at least) one carbanion-like intermediate of type I, which is thought[20] to

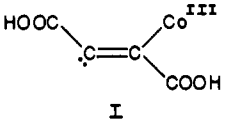

I

preserve its geometric configuration during reaction. A corresponding intermediate may be envisaged for reduction of the alkyne ester and, by implication, for the alkene esters as well, although with the latter the carbanion center would involve a σ-bonded carbon and need therefore not maintain its structural integrity.[21] A similar path (Scheme I) accommodates the $[H^+]$-proportional (k') path, but here the initial attack probably entails the "hydridic" hydrogen bound to cobalt. The Co(III) center freed in this step would not be expected to survive, for it has been shown[6a,22] to react very rapidly with Co(I) to yield Co(II), which is the observed corrin-bound cobalt product in all cases.

Acknowledgment. The authors are grateful to Professor R. N. Bose for help in computational procedures.

Registry No. cob(I)alamin, 13408-78-1; hydroxocobalamin hydrochloride, 59461-30-2; acetylenedicarboxylic acid dimethyl ester, 762-42-5; dimethyl fumarate, 624-49-7; dimethyl maleate, 624-48-6; diethyl maleate, 141-05-9; diethyl fumarate, 623-91-6; monoethyl fumarate, 2459-05-4.

(20) See, for example: (a) Nesmeyanov, A. N.; Borisov, A. E. *Tetrahedron*, **1957**, *1*, 157. (b) Dreiding, A. S.; Pratt, R. J. *J. Am. Chem. Soc.* **1954**, *76*, 1902. (c) Zweifel, G.; Lewis, W. *J. Org. Chem.* **1978**, *43*, 2793.
(21) See, for example: (a) Cram, D. J.; Nielsen, W. E.; Rickborn *J. Am. Chem. Soc.* **1960**, *82*, 6416. (b) Cram, D. J.; Nielsen, W. D. *J. Am. Chem.* **1961**, *83*, 2174.
(22) Ryan, D. A.; Espenson, J. H.; Meyerstein, D.; Mulac, W. A. *Inorg. Chem.* **1978**, *17*, 3725.

Contribution from the Institut für Anorganische Chemie and the Laboratorium für Kristallographie, Universität Bern, CH-3009 Bern, Switzerland

$[(phen)_2Mn^{IV}(\mu\text{-}O)_2Mn^{III}(phen)_2](PF_6)_3\cdot CH_3CN$ and $[(phen)_2Mn^{IV}(\mu\text{-}O)_2Mn^{IV}(phen)_2](ClO_4)_4\cdot CH_3CN$ (phen = 1,10-Phenanthroline): Crystal Structure Analyses at 100 K, Interpretation of Disorder, and Optical, Magnetic, and Electrochemical Results

M. Stebler,[1a,b] A. Ludi,[1a] and H.-B. Bürgi*[1b]

Received June 6, 1986

The crystal and molecular structures of the following two compounds have been determined: $[(phen)_2Mn^{IV}(\mu\text{-}O)_2Mn^{IV}(phen)_2](ClO_4)_4\cdot CH_3CN$ ($[1](ClO_4)_4\cdot CH_3CN$, phen = 1,10-phenanthroline: monoclinic, $P2_1/c$, a = 12.218 (7) Å, b = 29.431 (9) Å, c = 14.987 (7) Å, β = 112.22 (5)°, Z = 4) and $[(phen)_2Mn^{III}(\mu\text{-}O)_2Mn^{IV}(phen)_2](PF_6)_3\cdot CH_3CN$ ($[1](PF_6)_3\cdot CH_3CN$: orthorhombic, $Pbcn$, a = 9.891 (3) Å, b = 22.690 (3) Å, c = 22.858 (8) Å, Z = 4). In the former complex cation $[1]^{4+}$, the average distance of the Mn–N bonds perpendicular to the central MnO_2Mn ring (2.010 Å) is 0.066 Å shorter than the average distance of the Mn–N bonds in the plane of the ring, indicating a trans influence of O on N. In the latter complex cation $[1]^{3+}$, an average structure, with two crystallographically equivalent Mn ions, is found. Detailed analysis of anisotropic atomic displacement parameters (temperature factors) indicates either static or dynamic disorder between a Mn(III)–Mn(IV) and a Mn(IV)–Mn(III) ion. An optical absorption is observed for $[1]^{3+}$ at ~800 nm which is tentatively assigned as intervalence transition since its intensity is observed to increase with decreasing temperature. The exchange coupling constants for $[1]^{3+}$ and $[1]^{4+}$ (J = −148 (12) and −144 (3) cm^{-1}) are almost equal. The comproportionation constant obtained from cyclic voltammetry for the reaction Mn(IV)–Mn(IV) + Mn(III)–Mn(III) → 2(Mn(III)–Mn(IV)) is $\sim 10^{16}$.

Introduction

The mixed-valence complexes $[(phen)_2Mn^{III}(\mu\text{-}O)_2Mn^{IV}(phen)_2]^{3+}$ ($[1]^{3+}$, phen = 1,10-phenanthroline) and $[(bpy)_2Mn^{III}(\mu\text{-}O)_2Mn^{IV}(bpy)_2]^{3+}$ ($[2]^{3+}$, bpy = 2,2′-bipyridine) are believed to be model compounds for Mn-containing species occurring in photosynthesis.[2] Solution chemistry,[3] infrared,[3] optical,[3] and EPR[4] spectra, magnetism,[4,5] and electrochemistry[3,6] have been studied for the perchlorate salts of $[1]^{3+}$ and $[2]^{3+}$. According to the classification by Robin and Day[7] both ions are believed to be class II mixed-valence complexes. Indeed, the crystal structure of $[2](ClO_4)_3\cdot 3H_2O$ shows two structurally inequivalent metal ions.[5] EXAFS studies,[2] calibrated with the known structure of $[2]^{3+}$, show that the dimensions of the central Mn_2O_2 four-membered ring are very similar in $[1]^{3+}$ and $[1]^{4+}$.

In this work the crystal structures of the mixed-valence compound $[1](PF_6)_3\cdot CH_3CN$ and of its oxidized form $[1](ClO_4)_4\cdot C$-

(1) (a) Institut für Anorganische Chemie. (b) Laboratorium für Kristallographie.
(2) Kirby, J. A.; Robertson, A. S.; Smith, J. P.; Thompson, A. C.; Cooper, S. R.; Klein, M. P. *J. Am. Chem. Soc.* **1981**, *103*, 5529.
(3) Cooper, S. R.; Calvin, M. *J. Am. Chem. Soc.* **1977**, *99*, 6623.
(4) Cooper, S. R.; Dismukes, G. C.; Klein, M. P.; Calvin, M. *J. Am. Chem. Soc.* **1978**, *100*, 7248.
(5) Plaksin, P. M.; Stoufer, R. C.; Mathew, M.; Palenik, G. J. *J. Am. Chem. Soc.* **1972**, *94*, 2121. Plaksin, P. M. Ph.D. Thesis, University of Waterloo, Waterloo, Canada, 1971.
(6) Morrison, M. M.; Sawyer, D. T. *J. Am. Chem. Soc.* **1977**, *99*, 257.
(7) Robin, M. B.; Day, P. *Adv. Inorg. Chem. Radiochem.* **1967**, *10*, 247.

0020-1669/86/1325-4743$01.50/0

Table I. Crystal Data

$[(phen)_2Mn^{III}O_2Mn^{IV}(phen)_2](PF_6)_3 \cdot CH_3CN$			
formula	$Mn_2O_2N_9C_{50}H_{35}P_3F_{18}$		
mol wt	1338.7		
space group	Pbcn (No. 60)		
temp, K	100	200	298
a, Å	9.891 (3)	9.969 (3)	10.035 (2)
b, Å	22.690 (9)	22.726 (7)	22.756 (8)
c, Å	22.858 (8)	22.990 (8)	23.115 (6)
α, deg	90.0	90.0	90.0
β, deg	90.0	90.0	90.0
γ, deg	90.0	90.0	90.0
V, Å^3	5130 (3)	5207 (3)	5278 (3)
ΔV, %	−2.81	−1.34	
Z	4	4	4
ρ_{expt}, g/cm^3			1.66 (2)
ρ_{calcd}, g/cm^3			1.68
μ(Mo), cm^{-1}	7.4	7.4	7.4
F(000)	2864	2864	2864

$[(phen)_2Mn^{IV}O_2Mn^{IV}(phen)_2](ClO_4)_4 \cdot CH_3CN$		
formula	$Mn_2O_{18}N_9C_{50}H_{35}Cl_4$	
mol wt	1301.6	
space group	$P2_1/c$ (No. 14)	
temp, K	100	298
a, Å	12.218 (7)	12.516 (5)
b, Å	29.431 (9)	29.353 (10)
c, Å	14.987 (7)	15.022 (3)
α, deg	90.0	90.0
β, deg	112.22 (5)	111.48 (5)
γ, deg	90.0	90.0
V, Å^3	4989 (4)	5135 (3)
ΔV, %	−2.84	
Z	4	4
ρ_{expt}, g/cm^3		1.66 (2)
ρ_{calcd}, g/cm^3		1.68
μ(Mo), cm^{-1}	8.1	8.1
F(000)	2640	2640

H_3CN are described and compared; their magnetic susceptibilities, exchange couplings, the temperature dependence of the suspected intervalence transition in $[1]^{3+}$, and electrochemical results are also reported and (re)interpreted.

Experimental Section

Synthesis and Crystallization. $[1](PF_6)_3 \cdot CH_3CN$ was synthesized as described in ref 8. The olive powder thus obtained was redissolved in CH_3CN, filtered, and recrystallized in a desiccator. Green-black, air-stable crystals of octahedral shape were obtained. Anal. Calcd: Mn, 8.21; C, 44.86; N, 9.42; P, 6.94; F, 25.55; H, 2.64. Found: Mn, 8.39; C, 44.53; N, 9.06; P, 6.94; F, 25.81; H, 2.73; H_2O, 0.37.

$[1](ClO_4)_4 \cdot CH_3CN$ was synthesized as described in ref 9. The red-brown powder thus obtained was redissolved in absolute CH_3CN under N_2, filtered, and recrystallized in a desiccator at 30 °C. Dark red, air-stable cubes were obtained. Anal. Calcd: Mn, 8.44; C, 46.14; N, 9.69; Cl, 10.90; H, 2.71. Found: Mn, 8.04; C, 46.01; N, 9.62; Cl, 10.55; H, 2.86; H_2O, <0.5.

Magnetic susceptibilities in the temperature range 4–300 K were measured on freshly powdered samples by the Faraday method. Each measurement was done three times. The error in χ_{eff} is 0.5%. Diamagnetic corrections were calculated from standard values.[10]

Optical spectroscopy was performed with a Cary 17 instrument on films. The methyl acrylate "Degalan" (Fluka Co.) was stirred with CH_3CN under argon, $[1](PF_6)_3 \cdot CH_3CN$ was dissolved in it, and the slurry was poured into a Petri dish. On evaporation of the solvent transparent films were obtained.

Cyclic voltammetry was performed with a scanner E-612 and detector E-611 (Metrohm Co.) by the usual three-electrode method. Pt electrodes were used, and the reference was Ag/AgCl; the 50-mL container was kept under argon; the solvent was CH_3CN and the electrolyte 0.1 M $(NBu_4)ClO_4$.

Diffraction Measurements and Crystal Data. The crystal data of $[1](PF_6)_3 \cdot CH_3CN$ and $[1](ClO_4)_4 \cdot CH_3CN$ are summarized in Table I.

Table II. Data Collection and Data Reduction

	$[1](PF_6)_3 \cdot CH_3CN$	
cryst dimens, mm^3	0.27 × 0.20 × 0.15	0.27 × 0.20 × 0.15
temp, K	200	100
θ limits, deg	0–25	0–26
scan width, deg	0.95 + 0.4 tan θ	0.95 + 0.4 tan θ
mode	ω mode, variable scan speed	ω mode, variable scan speed
max scan time, s	240	240
h,k,l (min→max)	0→11, 0→27, 0→27	0→12, 0→28, 0→28
transmissn factors, min/max	0.80/0.90	0.80/0.90
$\sigma(I)/I \geq$	0.04	0.04
no. of unique reflctns measd	4575	5027
no. of reflctns with $F_o^2 > 3\sigma(F_o^2)$	2261	2845
no. of parameters	408	408
R	0.037	0.035
R_w	0.038	0.039

	$[1](ClO_4)_4 \cdot CH_3CN$
cryst dimens, mm^3	0.22 × 0.22 × 0.25
temp, K	100
θ limits, deg	0–25
scan width, deg	0.9 + 0.5 tan θ
mode	ω mode, variable scan speed
max scan time, s	240
h,k,l (min→max)	−14→14, 0→35, 0→17
transmissn factors, min/max	0.76/0.89
$\sigma(I)/I \geq$	0.04
no. of unique reflctns measd	8747
no. of reflctns with $F_o^2 > 3\sigma(F_o^2)$	6102
no. of parameters	784
R	0.035
R_w	0.038

A dark green crystal of $[1](PF_6)_3 \cdot CH_3CN$ with pyramidal shape and a red, cube-shaped crystal of $[1](ClO_4)_4 \cdot CH_3CN$ were chosen for X-ray diffraction experiments. Space groups were determined from preliminary precession photographs. The unit-cell and intensity data were measured with a CAD-4 diffractometer (Enraf-Nonius) equipped with a liquid-nitrogen-cooling device. Graphite-monochromated Mo Kα radiation (λ = 0.71069 Å) was used. The cell constants were determined from 14 reflections in the ranges 11° < θ < 19° ($[1](ClO_4)_4 \cdot CH_3CN$) and 10.5° < θ < 16.5° ($[1](PF_6)_3 \cdot CH_3CN$) at several temperatures between 298 K and 100 K. The uncertainties in the temperature measurements were <10 K.

The parameters of data collection are listed in Table II. The structure of $[1](PF_6)_3 \cdot CH_3CN$ was initially measured at 200 K. It showed a strong disorder of a PF_6 anion which could not be resolved. Therefore a second data set was measured at 100 K on the same crystal. During data collection three control reflections were measured every 3 h; the crystal of $[1](PF_6)_3 \cdot CH_3CN$ was stable, and the check reflections of $[1](ClO_4)_4 \cdot CH_3CN$ showed a slight decay in intensity of 4.7% during the X-ray exposure time of 182 h. Diffracted intensities were corrected for decay ($[1](ClO_4)_4 \cdot CH_3CN$) and for Lorentz and polarization effects, but not for absorption. The maximal and minimal transmission factors were estimated for the two crystals from the crystal dimensions (Table II). For all non-hydrogen atoms, neutral atom scattering factors, including anomalous dispersion corrections ($\Delta f'$, $\Delta f''$), were used.[11]

Data reduction was performed, with the "Structure Determination Package" from Enraf-Nonius[12] on a PDP11/34 computer. The solution and refinement of the structures were performed on an IBM-3033 computer by using the SHELX-76 program system.[13] The drawings were prepared with ORTEP of the XRAY-76 system.[14]

Solution and Refinement of the Structures. $[1](ClO_4)_4 \cdot CH_3CN$. The Mn atoms were located from a Patterson map. In two subsequent difference Fourier syntheses, all non-hydrogen atoms were detected. Fur-

(8) Uson, R.; Riera, V.; Ciriano, M. *Transition Met. Chem.* **1976**, *1*, 98.
(9) Goodwin, H. A.; Sylva, R. N. *Aust. J. Chem.* **1967**, *20*, 629.
(10) Landolt-Börnstein, Neue Serie II, 1976, Vol. 10.
(11) *International Tables for X-Ray Crystallography*; Kynoch: Birmingham, 1974; Vol. IV, Tables 2.2B and 2.3.1 (present distributor D. Reidel, Dortrecht).
(12) Frenz, B. A. Structure Determination Package; Texas A&M University: College Station, TX, and Enraf-Nonius: Delft, 1983.
(13) Sheldrick, G. M. SHELX76, Program for Crystal Structure Determination; University of Cambridge: Cambridge, England, 1976.
(14) Steward, J. M. XRAY76; Computer Science Center, University of Maryland: College Park, MD, 1976.

Table III. Final Atomic Coordinates and B_{eq} Values of $[(phen)_2Mn^{IV}(\mu\text{-}O)_2Mn^{IV}(phen)_2](ClO_4)_4\cdot CH_3CN$ at 100 K[a]

atom	x/a	y/b	z/c	B_{eq},[b] Å^2	atom	x/a	y/b	z/c	B_{eq},[b] Å^2
Mn1	−0.14575 (5)	0.12104 (2)	0.20761 (4)	0.91 (1)	C311	−0.2148 (3)	0.1498 (1)	0.3578 (2)	1.06 (8)
Mn2	0.09681 (5)	0.12303 (2)	0.28766 (4)	0.95 (1)	C312	−0.2693 (3)	0.1820 (1)	0.2839 (2)	0.90 (8)
O1	−0.0262 (2)	0.16159 (7)	0.2447 (2)	1.07 (5)	C313	−0.3240 (3)	0.2205 (1)	0.3027 (3)	1.19 (8)
O2	−0.0223 (2)	0.08263 (8)	0.2494 (2)	1.12 (5)	C314	−0.2168 (3)	0.1553 (1)	0.4504 (2)	1.12 (8)
N101	−0.2561 (2)	0.0666 (1)	0.1437 (2)	1.07 (7)	N401	0.2146 (3)	0.1754 (1)	0.2939 (2)	1.22 (7)
N201	0.2095 (2)	0.0709 (1)	0.3593 (2)	1.07 (7)	C402	0.2625 (3)	0.2066 (1)	0.3610 (3)	1.70 (9)
C102	−0.3074 (3)	0.0369 (1)	0.1811 (3)	1.50 (9)	C403	0.3242 (3)	0.2441 (1)	0.3457 (3)	1.97 (10)
C103	−0.3602 (3)	−0.0027 (1)	0.1315 (3)	1.67 (9)	C404	0.3364 (3)	0.2496 (1)	0.2598 (3)	2.04 (10)
C104	−0.3569 (3)	−0.0124 (1)	0.0437 (3)	1.40 (9)	C405	0.3020 (4)	0.2170 (1)	0.0965 (3)	2.32 (10)
C105	−0.2980 (3)	0.0138 (1)	−0.0918 (3)	1.45 (9)	C406	0.2610 (4)	0.1825 (1)	0.0325 (3)	2.39 (11)
C106	−0.2501 (3)	0.0461 (1)	−0.1295 (3)	1.59 (9)	C407	0.1576 (3)	0.1074 (1)	−0.0081 (3)	1.91 (10)
C107	−0.1580 (3)	0.1241 (1)	−0.1131 (3)	1.67 (9)	C408	0.0990 (3)	0.0733 (1)	0.0180 (3)	1.49 (9)
C108	−0.1178 (3)	0.1619 (1)	−0.0569 (3)	1.59 (9)	C409	0.0808 (3)	0.0763 (1)	0.1041 (2)	1.24 (9)
C109	−0.1178 (3)	0.1632 (1)	0.0357 (3)	1.18 (8)	N410	0.1212 (3)	0.1116 (1)	0.1637 (2)	1.16 (7)
N110	−0.1595 (2)	0.1289 (1)	0.0714 (2)	0.98 (7)	C411	0.1829 (3)	0.1450 (1)	0.1401 (3)	1.18 (8)
C111	−0.2061 (3)	0.0922 (1)	0.0145 (2)	0.92 (8)	C412	0.2300 (3)	0.1802 (1)	0.2082 (3)	1.28 (8)
C112	−0.2559 (3)	0.0580 (1)	0.0540 (2)	0.91 (8)	C413	0.2902 (3)	0.2164 (1)	0.1877 (3)	1.64 (9)
C113	−0.3046 (3)	0.0189 (1)	0.0010 (3)	1.15 (8)	C414	0.2009 (3)	0.1449 (1)	0.0529 (3)	1.72 (9)
C114	−0.2037 (3)	0.0876 (1)	−0.0777 (3)	1.32 (9)	Cl1	0.00668 (8)	0.46072 (3)	0.24581 (6)	1.54 (2)
C202	0.2531 (3)	0.0371 (1)	0.3245 (3)	1.44 (9)	O11	0.0234 (4)	0.4883 (1)	0.3291 (2)	3.57 (9)
C203	0.3220 (3)	0.0028 (1)	0.3827 (3)	1.69 (9)	O12	0.0986 (3)	0.4275 (1)	0.2699 (2)	3.33 (9)
C204	0.3456 (3)	0.0022 (1)	0.4796 (3)	1.71 (9)	O13	−0.1049 (3)	0.4381 (1)	0.2173 (2)	3.01 (8)
C205	0.3178 (3)	0.0408 (1)	0.6195 (3)	1.53 (9)	O14	0.0076 (3)	0.4886 (1)	0.1671 (2)	3.00 (8)
C206	0.2704 (3)	0.0747 (1)	0.6525 (3)	1.72 (9)	Cl2	−0.04652 (9)	0.28374 (3)	0.24339 (7)	1.82 (2)
C207	0.1500 (3)	0.1464 (1)	0.6181 (3)	1.58 (9)	O21	−0.1394 (3)	0.3170 (1)	0.2113 (2)	3.19 (9)
C208	0.0857 (3)	0.1781 (1)	0.5508 (3)	1.43 (9)	O22	−0.0497 (4)	0.2580 (1)	0.1616 (2)	4.40 (11)
C209	0.0684 (3)	0.1722 (1)	0.4540 (3)	1.13 (8)	O23	−0.0680 (3)	0.2547 (1)	0.3122 (2)	2.73 (8)
N210	0.1138 (2)	0.1365 (1)	0.4243 (2)	1.02 (7)	O24	0.0632 (3)	0.3065 (1)	0.2869 (3)	4.77 (12)
C211	0.1817 (3)	0.1061 (1)	0.4913 (3)	1.07 (8)	Cl3	0.48498 (8)	0.36692 (3)	0.39018 (7)	1.53 (2)
C212	0.2318 (3)	0.0703 (1)	0.4559 (2)	1.07 (8)	O31	0.5193 (3)	0.3815 (1)	0.4892 (2)	2.95 (8)
C213	0.2998 (3)	0.0369 (1)	0.5190 (3)	1.33 (8)	O32	0.5537 (3)	0.3277 (1)	0.3880 (2)	2.93 (8)
C214	0.1996 (3)	0.1094 (1)	0.5889 (3)	1.27 (8)	O33	0.5080 (3)	0.4030 (1)	0.3357 (2)	2.93 (8)
N301	−0.2662 (3)	0.1723 (1)	0.1959 (2)	1.08 (7)	O34	0.3613 (2)	0.3559 (1)	0.3511 (2)	2.29 (7)
C302	−0.3242 (3)	0.1998 (1)	0.1230 (3)	1.37 (9)	Cl4	0.49090 (9)	0.09848 (4)	0.30973 (8)	2.46 (3)
C303	−0.3823 (3)	0.2385 (1)	0.1350 (3)	1.59 (9)	O41	0.3986 (3)	0.0762 (1)	0.2342 (2)	3.70 (9)
C304	−0.3810 (3)	0.2497 (1)	0.2248 (3)	1.53 (9)	O42	0.5985 (3)	0.0736 (1)	0.3403 (3)	3.44 (9)
C305	−0.3210 (3)	0.2268 (1)	0.3989 (3)	1.62 (9)	O43	0.4582 (3)	0.1031 (2)	0.3919 (3)	6.07 (13)
C306	−0.2693 (3)	0.1960 (1)	0.4689 (3)	1.58 (9)	O44	0.5084 (3)	0.1425 (1)	0.2778 (4)	5.58 (14)
C307	−0.1661 (3)	0.1204 (1)	0.5173 (3)	1.37 (8)	N1	0.4115 (3)	0.3250 (1)	0.0814 (3)	2.37 (9)
C308	−0.1193 (3)	0.0831 (1)	0.4905 (3)	1.23 (8)	C1	0.4875 (4)	0.3501 (1)	0.1037 (3)	2.00 (10)
C309	−0.1166 (3)	0.0806 (1)	0.3986 (3)	1.16 (8)	C2	0.5853 (4)	0.3814 (2)	0.1346 (4)	3.65 (14)
N310	−0.1620 (2)	0.1137 (1)	0.3345 (2)	1.00 (7)					

[a] Atomic numbering is shown in Figure 1. [b] For anisotropically refined atoms the isotropic equivalent displacement parameter is given in the form $B_{eq} = 8\pi^2U_{eq} = (^8/_3)\pi^2\sum_i\sum_j U_{ij}a_ia_j(a_i\cdot a_j)$, where the general temperature factor expression is $\exp[-2\pi^2(U_{11}h^2a^{*2} + U_{22}k^2b^{*2} + U_{33}l^2c^{*2} + 2U_{12}hka^*b^* + 2U_{13}hla^*c^* + 2U_{23}klb^*c^*)]$.

thermore, the presence of one molecule of acetonitrile was revealed, which had not been recognized in the initial interpretation of the chemical analysis. Non-hydrogen atoms were refined anisotropically. Hydrogen atoms were fixed at calculated positions (d(C–H) = 0.93 Å); their isotropic displacement parameters were refined individually. Since the number of parameters (748) exceeds the maximum allowed by the program, every cycle of least-squares refinement had to be done in two steps. During each step half of the binuclear cation and two anions were refined. The final positional parameters had shift/error ratios less than 0.1, and the scaling factor and some of the displacement parameters of oxygen and hydrogen atoms showed shift/error ratios in the range of 0.1–0.3; the largest correlation between two parameters was 0.55. Unit weights were used with the minimization function $\sum w(|F_o| - |F_c|)^2$ and led to satisfactorily constant values of the minimization function for subsets of reflections in ranges of $(\sin\theta)/\lambda$, F_o, h, k, and l. In the final difference Fourier synthesis the minimum and maximum electron densities were −0.45 and 0.64 e/Å^3, respectively. The largest residual electron density was in the neighborhood of anions 2 and 4, suggesting slight disorder. This is also indicated by the large displacement parameters for some of their oxygen atoms.

Final atomic positions and equivalent isotropic displacement parameters of all non-hydrogen atoms are listed in Table III.

[1](PF$_6$)$_3$·CH$_3$CN. The position of the Mn atom was determined from a Patterson map, computed with the data set collected at 200 K. In a sequence of difference Fourier syntheses and two cycles of least-squares refinement the whole binuclear molecule, one PF_6^- in general position, and an anion, [PF_6(**2**)], lying on a twofold axis were found. The displacement parameters of the latter did not converge; a ΔF map revealed disorder. A second anion, [PF_6(**3**)], but with a much smaller occupation factor (≃20%) was also observed on the twofold axis; its fluorine atoms could not be resolved. Several cycles of refinement with isotropic displacement parameters for [PF_6(**2**)] and [PF_6(**3**)] and anisotropic ones for all other non-hydrogen atoms reduced the R value to 0.064. Some electron density (∼1.5 e/Å^3) on the twofold axis, at 1 Å from the phosphorus atom of [PF_6(**3**)], could not be explained.

Interpretation of the data set collected at 100 K was based on the positional parameters of the binuclear molecule and PF_6^- in general position obtained at 200 K. A difference Fourier synthesis again showed two disordered anions, [PF_6(**2**)] and [PF_6(**3**)]. In addition, CH_3CN lying in approximately the same positions as the anions was detected. As in the structure of [**1**](ClO$_4$)$_4$·CH$_3$CN, acetonitrile had not been observed in the initial interpretation of the chemical analysis; however, the agreement between experimental and calculated elemental compositions improved after CH_3CN was taken into account. The following model of disorder was used for further refinement: [PF_6(**3**)] was modeled with constrained P–F and F···F distances and a single isotropic displacement parameter for the fluorine atoms. Moreover, it was assumed that each of the two sites showing disorder is occupied by either PF_6^- or CH_3CN; therefore only one occupation factor is needed. All other non-hydrogen atoms were refined anisotropically, while the hydrogen atoms were placed in calculated positions, d(C–H) = 0.95 Å, with adjustable isotropic displacement parameters. R dropped to 0.043. In the final refinement the distance constraints were relaxed and the structure was refined to convergence. For the three fluorine atoms of [PF_6(**3**)] only one isotropic displacement parameter was refined.

The result of this procedure is as follows: (1) [PF_6(**2**)] with anisotropically refined fluorine atoms lies on a twofold axis (site occupation factor of 0.805 (4)). The geometry of this anion shows no unusual feature (compared with PF_6^- in general position). (2) [PF_6(**3**)] lies on a twofold axis with an occupation factor of 0.195. The common isotropic

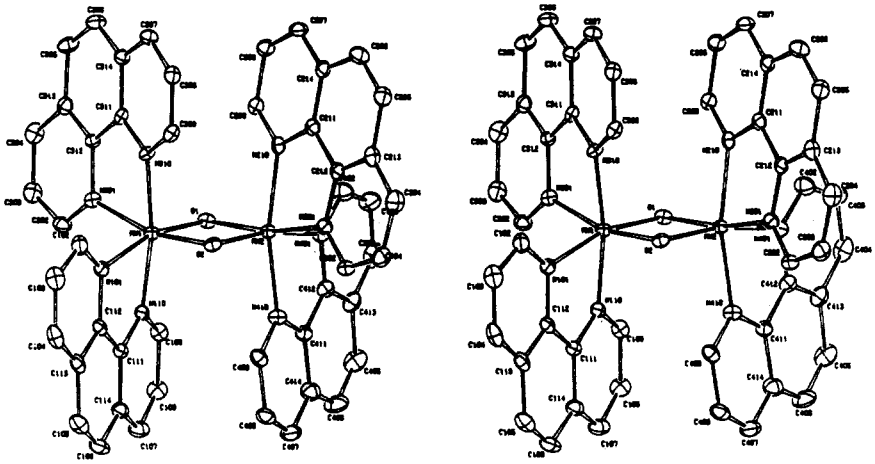

Figure 1. Stereo drawing of a molecule of $[1]^{4+}$ showing the numbering scheme of the complex. Thermal ellipsoids are drawn at the 50% probability level.

displacement parameter of the fluorine atoms is big. (3) [CH_3CN(2)], with a site occupation factor of 0.195, lies along a twofold axis. The central carbon atom C21 coincides with the phosphorus atom of [PF_6(2)]. (4) [CH_3CN(3)], with population 0.403, meets the twofold axis at an angle of 30 (1)°. C32 is displaced along the twofold axis by ~1 Å from the phosphorus atom of [PF_6(3)].

The binuclear molecule and PF_6^- in general position do not seem to be strongly affected by the model used to describe disorder; their positional parameters differ less than a standard deviation for various models of disorder. Unit weights were used and led to satisfactorily constant values of the minimization function for subsets of reflections in ranges of $(\sin\theta)/\lambda$, F_o, h, k, and l. The largest shift/error ratio was 0.03. In the final ΔF map the largest features in electron density were −0.37 and 0.48 e/Å^3. All of the remaining electron density is found in the neighborhood of the disordered PF_6^- anion and CH_3CN. The same model was used to refine the structure measured at 200 K. The largest feature in the difference Fourier map was 0.49 e/Å^3. In Table IV positional and isotropic equivalent displacement parameters of the non-hydrogen atoms are listed.

A comparison of the structures of $[1](PF_6)_3\cdot CH_3CN$, measured at 100 and 200 K and refined with the same model, shows large differences in the atomic parameters. The coordinates of the heavier atoms (Mn, P) differ by more than 10 standard deviations due to the anisotropic change of the cell parameters (Table I). The difference in displacement parameters is obviously due to the difference in temperature. An alternative indicator for the differences between the two structures are internal parameters. However, bond lengths and angles of the two structures are the same to within one standard deviation.

Results

Description of the Structures. $[1](ClO_4)_4\cdot CH_3CN$. The asymmetric unit contains one binuclear ion, four ClO_4^- anions, and one CH_3CN. The site symmetry of the binuclear ion is 1. Distances and angles pertaining to the inner coordination of Mn are listed in Table V; the molecule is shown in Figure 1. The central unit of the complex ion is a planar four-membered ring consisting of two Mn atoms and two bridging O atoms. The largest deviation from the least-squares plane is less than 0.006 Å. The Mn–Mn and O–O distances are 2.748 (2) and 2.326 (4) Å, respectively, indicating no significant metal-to-metal bond.

Two phen ligands complete the coordination (roughly octahedral) around each Mn. The eight independent Mn–N bond lengths show an average value of 2.043 (13) Å. The average Mn1–N distance (2.037 (22) Å) is equal to the average Mn2–N distance (2.049 (17) Å), which suggests that the coordination geometries of the two manganese atoms are virtually identical; the average Mn–O distances are 1.802 (3) and 1.798 (1) Å, respectively. For both Mn's the average equatorial Mn–N distance (2.076 (4) Å) is significantly longer than the average axial Mn–N distance (2.010 (6) Å); this reflects the trans influence of the two bridging oxygen atoms on the equatorial nitrogen atoms.

In the structure of $[(bpy)_2Mn^{III}(\mu\text{-}O)_2Mn^{IV}(bpy)_2]^{3+}$ ([2]-$(ClO_4)_3\cdot 3H_2O$; Table V), studied at room temperature, the geometries of the two manganese atoms are distinctly different, indicating one Mn(IV) and one Mn(III) ion;[5] since the bond

Table IV. Final Atomic Coordinates and B_{eq} Values[a] of $[(phen)_2Mn^{III}(\mu\text{-}O)_2Mn^{IV}(phen)_2](PF_6)_3\cdot CH_3CN$ at 100 K

atom	x/a	y/b	z/c	B_{eq},[b] Å^2
Mn	0.4830 (1)	0.26019 (2)	0.69144 (3)	1.10 (3)
O	0.3782 (3)	0.2614 (1)	0.7570 (1)	1.59 (13)
N101	0.3184 (3)	0.2376 (2)	0.6387 (1)	1.45 (16)
C102	0.2186 (4)	0.2721 (2)	0.6212 (2)	2.22 (20)
C103	0.1043 (5)	0.2506 (2)	0.5919 (2)	2.97 (24)
C104	0.0934 (5)	0.1920 (2)	0.5799 (2)	1.69 (24)
C105	0.1989 (5)	0.0919 (2)	0.5847 (2)	1.73 (24)
C106	0.3037 (6)	0.0579 (2)	0.6021 (2)	2.44 (25)
C107	0.5246 (6)	0.0489 (2)	0.6552 (2)	4.47 (26)
C108	0.6266 (5)	0.0758 (2)	0.6858 (2)	4.94 (26)
C109	0.6188 (5)	0.1365 (2)	0.6967 (2)	3.33 (23)
N110	0.5158 (4)	0.1685 (1)	0.6775 (1)	2.17 (17)
C111	0.4152 (4)	0.1422 (2)	0.6468 (2)	1.69 (19)
C112	0.3079 (5)	0.1783 (2)	0.6271 (2)	1.60 (19)
C113	0.1978 (5)	0.1540 (2)	0.5967 (2)	1.60 (21)
C114	0.4151 (5)	0.0813 (2)	0.6345 (2)	2.65 (22)
N201	0.6119 (3)	0.2814 (1)	0.6203 (1)	1.27 (15)
C202	0.6859 (4)	0.2458 (2)	0.5875 (2)	1.81 (19)
C203	0.7795 (4)	0.2660 (2)	0.5460 (2)	2.09 (20)
C204	0.8010 (5)	0.3257 (2)	0.5402 (2)	2.26 (21)
C205	0.7336 (5)	0.4279 (2)	0.5688 (2)	1.87 (23)
C206	0.6512 (6)	0.4633 (2)	0.5990 (2)	2.07 (24)
C207	0.4558 (6)	0.4740 (2)	0.6690 (2)	2.58 (25)
C208	0.3621 (6)	0.4477 (2)	0.7037 (2)	2.64 (27)
C209	0.3623 (5)	0.3861 (2)	0.7097 (2)	2.36 (24)
N210	0.4505 (4)	0.3522 (1)	0.6811 (1)	1.30 (16)
C211	0.5414 (4)	0.3785 (2)	0.6447 (2)	1.30 (19)
C212	0.6284 (4)	0.3409 (2)	0.6121 (2)	1.17 (18)
C213	0.7235 (4)	0.3650 (2)	0.5733 (2)	1.37 (20)
C214	0.5492 (5)	0.4401 (2)	0.6378 (2)	1.53 (21)
P1	0.7439 (1)	0.0977 (1)	0.4896 (1)	2.76 (6)
F11	0.7914 (3)	0.1068 (1)	0.5562 (1)	3.42 (14)
F12	0.6969 (4)	0.0903 (1)	0.4230 (1)	2.77 (16)
F13	0.8511 (3)	0.1476 (1)	0.4696 (1)	3.47 (14)
F14	0.8560 (3)	0.0485 (1)	0.4806 (1)	6.12 (16)
F15	0.6309 (3)	0.1478 (1)	0.4984 (1)	2.85 (14)
F16	0.6381 (3)	0.0488 (1)	0.5097 (1)	3.56 (15)
P2	0.5000 (0)	0.3616 (1)	0.2500 (0)	1.83 (6)*
F21	0.6079 (3)	0.3117 (1)	0.2670 (1)	4.02 (17)
F22	0.4437 (3)	0.3614 (2)	0.3150 (1)	3.98 (18)
F23	0.6089 (4)	0.4102 (2)	0.2669 (2)	2.21 (19)
P3	0.5000 (0)	0.1198 (5)	0.2500 (0)	2.74 (21)*
F31	0.4020 (33)	0.0700 (13)	0.2724 (12)	9.94 (52)*
F32	0.5601 (30)	0.1133 (12)	0.3135 (13)	9.94 (52)*
F33	0.4177 (37)	0.1782 (16)	0.2671 (15)	9.94 (52)*
N2	0.5000 (0)	0.4010 (34)	0.2500 (0)	9.52 (167)*
C21	0.5000 (0)	0.3466 (15)	0.2500 (0)	0.09 (66)*
C22	0.5000 (0)	0.2849 (26)	0.2500 (0)	6.95 (136)*
N3	0.4285 (25)	0.1766 (10)	0.2962 (9)	8.91 (62)*
C31	0.4633 (30)	0.1288 (13)	0.2732 (12)	8.82 (68)*
C32	0.5000 (0)	0.0800 (7)	0.2500 (0)	6.28 (30)*

[a] Atomic numbering in Figure 2. [b] Atoms with an asterisk were refined isotropically. See footnote *b* in Table III.

Table V. Coordination Geometry and Difference Displacement Parameters of Dioxo-Bridged Manganese(IV)–Manganese(IV) and Manganese(III)–Manganese(IV) Complexes[a]

	[1](ClO$_4$)$_4$·CH$_3$CN 100 K		[1](PF$_6$)$_3$·CH$_3$CN 100 K			[1](ClO$_4$)$_4$·CH$_3$CN 100 K		[1](PF$_6$)$_3$·CH$_3$CN 100 K	
	dist[b]	ΔU_{obsd}[c]	dist	ΔU_{obsd}		dist[b]	ΔU_{obsd}[c]	dist	ΔU_{obsd}
Mn1–Mn2	2.748 (2)	3 (4)	2.700 (1)	0 (4)	Mn2–O1	1.798 (3)	18 (13)	1.820 (3)	56 (15)
O1–O2	2.326 (4)		2.422 (4)		Mn2–O2	1.797 (3)	27 (13)	1.808 (3)	17 (15)
Mn1–O1	1.805 (3)	14 (13)	1.808 (3)	17 (15)	Mn2–N2$_{eq}$	2.070 (3)	9 (16)	2.120 (3)	1 (18)
Mn1–O2	1.798 (3)	25 (13)	1.820 (3)	56 (15)	Mn2–N2$_{ax}$	2.020 (3)	72 (16)	2.128 (2)	129 (17)
Mn1–N1$_{eq}$	2.079 (3)	34 (16)	2.090 (3)	26 (17)	Mn2–N4$_{eq}$	2.087 (3)	42 (16)	2.090 (3)	26 (17)
Mn1–N1$_{ax}$	2.001 (3)	31 (15)	2.127 (2)	141 (17)	Mn2–N4$_{ax}$	2.020 (4)	31 (16)	2.127 (2)	141 (17)
Mn1–N3$_{eq}$	2.069 (3)	28 (16)	2.120 (3)	1 (18)					
Mn1–N3$_{ax}$	1.999 (3)	−2 (16)	2.128 (2)	129 (17)					

	[1](PF$_6$)$_3$·CH$_3$CN 200 K		[2](ClO$_4$)$_3$·3H$_2$O[d] 298 K			[1](PF$_6$)$_3$·CH$_3$CN 200 K		[2](ClO$_4$)$_3$·3H$_2$O[d] 298 K	
	dist	ΔU_{obsd}	dist	ΔU_{obsd}		dist	ΔU_{obsd}	dist	ΔU_{obsd}
Mn1–Mn2	2.695 (9)	0 (4)	2.716 (2)	−73 (66)	Mn2–O1	1.820 (5)	42 (20)	1.784 (5)	51 (43)
O1–O2	2.425 (8)		2.419 (8)		Mn2–O2	1.805 (5)	24 (19)	1.784 (5)	97 (44)
Mn1–O1	1.805 (5)	24 (19)	1.853 (6)	−31 (43)	Mn2–N2$_{eq}$	2.121 (6)	8 (25)	2.075 (8)	71 (61)
Mn1–O2	1.820 (5)	42 (20)	1.856 (6)	−55 (44)	Mn2–N2$_{ax}$	2.128 (9)	133 (22)	2.016 (7)	56 (47)
Mn1–N1$_{eq}$	2.093 (6)	52 (24)	2.129 (7)	−57 (191)	Mn2–N4$_{eq}$	2.093 (6)	52 (24)	2.075 (7)	60 (187)
Mn1–N1$_{ax}$	2.129 (9)	185 (22)	2.207 (7)	−23 (51)	Mn2–N4$_{ax}$	2.129 (9)	185 (22)	2.028 (7)	−7 (192)
Mn1–N3$_{eq}$	2.121 (6)	8 (25)	2.134 (7)	120 (124)					
Mn1–N3$_{ax}$	2.128 (9)	133 (22)	2.226 (7)	90 (191)					

Averaged Coordination Geometry

Distances, Å

	[1](ClO$_4$)$_4$·CH$_3$CN[e] 100 K	[1](PF$_6$)$_3$·CH$_3$CN[f] 100 K		[1](ClO$_4$)$_4$·CH$_3$CN[e] 100 K	[1](PF$_6$)$_3$·CH$_3$CN[f] 100 K
⟨Mn1–N$_{eq}$⟩	2.074 (5)	2.105 (15)	⟨Mn1–N⟩	2.037 (22)	2.116 (9)
⟨Mn1–N$_{ax}$⟩	2.000 (1)	2.128 (1)	⟨Mn2–N⟩	2.049 (17)	2.116 (9)
⟨Mn2–N$_{eq}$⟩	2.079 (9)	2.105 (15)	⟨Mn–N⟩	2.043 (13)	2.116 (6)
⟨Mn2–N$_{ax}$⟩	2.020 (1)	2.128 (1)	⟨Mn1–O⟩	1.802 (4)	1.814 (6)
⟨Mn–N$_{eq}$⟩	2.076 (4)	2.105 (9)	⟨Mn2–O⟩	1.798 (1)	1.814 (6)
⟨Mn–N$_{ax}$⟩	2.010 (6)	2.128 (1)	⟨Mn–O⟩	1.800 (2)	1.814 (4)

	[1](PF$_6$)$_3$·CH$_3$CN[f] 200 K	[2](ClO$_4$)$_3$·3H$_2$O[e] 298 K		[1](PF$_6$)$_3$·CH$_3$CN[f] 200 K	[2](ClO$_4$)$_3$·3H$_2$O[e] 298 K
⟨Mn1–N$_{eq}$⟩	2.107 (14)	2.132 (3)	⟨Mn1–N⟩	2.118 (8)	2.174 (25)
⟨Mn1–N$_{ax}$⟩	2.129 (1)	2.217 (10)	⟨Mn2–N⟩	2.118 (8)	2.049 (16)
⟨Mn2–N$_{eq}$⟩	2.107 (14)	2.075 (1)	⟨Mn–N⟩	2.118 (6)	2.111 (27)
⟨Mn2–N$_{ax}$⟩	2.129 (1)	2.022 (6)	⟨Mn1–O⟩	1.813 (8)	1.855 (2)
⟨Mn–N$_{eq}$⟩	2.107 (8)	2.103 (16)	⟨Mn2–O⟩	1.813 (8)	1.784 (1)
⟨Mn–N$_{ax}$⟩	2.129 (1)	2.119 (56)	⟨Mn–O⟩	1.813 (6)	1.819 (21)

Angles, deg

	[1](ClO$_4$)$_4$·CH$_3$CN[e] 100 K	[1](PF$_6$)$_3$·CH$_3$CN[f] 100 K		[1](ClO$_4$)$_4$·CH$_3$CN[e] 100 K	[1](PF$_6$)$_3$·CH$_3$CN[f] 100 K
O–Mn–O′	80.5 (1)	84.0 (1)	N$_{ax}$–Mn–N′$_{ax}$	168.4 (1.9)	165.1 (1)
Mn–O–Mn′	99.5 (2)	96.0 (1)	N$_{ax}$–Mn–N′$_{eq}$	91.4 (1.2)	90.9 (1)
N$_{ax}$–Mn–N$_{eq}$	80.1 (2)	77.8 (3)	N$_{eq}$–Mn–O	164.0 (4)	165.8 (2)
N$_{ax}$–Mn–O	89.0 (3)	89.6 (2)	N$_{eq}$–Mn–O′	89.9 (6)	92.1 (2)
N$_{ax}$–Mn–O′	99.9 (1.0)	101.4 (1.5)	N$_{eq}$–Mn–N′$_{eq}$	102.0 (2)	94.7 (1)

	[1](PF$_6$)$_3$·CH$_3$CN[f] 200 K	[2](ClO$_4$)$_3$·3H$_2$O[e] 298 K		[1](PF$_6$)$_3$·CH$_3$CN[f] 200 K	[2](ClO$_4$)$_3$·3H$_2$O[e] 298 K
O–Mn–O′	84.0 (1)	83.4 (2.8)	N$_{ax}$–Mn–N′$_{ax}$	164.9 (2)	161.3 (5.1)
Mn–O–Mn′	96.0 (3)	96.6 (1)	N$_{ax}$–Mn–N′$_{eq}$	91.3 (2)	90.3 (1.4)
N$_{ax}$–Mn–N$_{eq}$	77.6 (4)	77.1 (2.4)	N$_{eq}$–Mn–O	165.6 (3)	168.9 (1.8)
N$_{ax}$–Mn–O	89.7 (2)	93.7 (1)	N$_{eq}$–Mn–O′	92.2 (2)	92.3 (4)
N$_{ax}$–Mn–O′	101.6 (1.4)	100.3 (2.3)	N$_{eq}$–Mn–N′$_{eq}$	94.8 (3)	93.8 (1.4)

[a] Esd's in parentheses; calculated according to $\sigma = ((\sum \Delta x^2)/n(n-1))^{1/2}$. [b] Distances in Å. [c] ΔU's in Å^2 10^4. [d] Structural data from ref 5. [e] Assuming $2/m$ symmetry. [f] Assuming an additional mirror plane perpendicular to the twofold axis.

lengths around Mn(IV) are very similar to those found in $[(phen)_2Mn^{IV}(\mu\text{-}O)_2Mn^{IV}(phen)_2]^{4+}$ (Table V), either one or the other of two conclusions is possible: (1) If it is assumed that in $[(bpy)_2Mn^{III}(\mu\text{-}O)_2Mn^{IV}(bpy)_2]^{3+}$ the two manganese ions are not influencing each others coordination geometry, it may be concluded that phen and bpy show very similar coordination to Mn(IV). Also the influence of the temperature would seem to be negligible. (2) If we assume that there is no difference in coordination geometry of bpy and phen at Mn(IV), then the mixed-valence compound [2](ClO$_4$)$_3$·3H$_2$O is perfectly localized and therefore no averaging of the coordination geometry of the two metal centers is seen.

Averaged distances and bond angles of the four independent phenanthrolines were calculated by assuming $2/m$ symmetry of the complex and are given in Table VI. Corresponding average bond lengths of the ligands in the two binuclear manganese complexes differ only insignificantly. Phen 2 is almost planar (largest deviation: 0.045 Å of N210); atoms C*i*03, C*i*07, C*i*08, and especially N*i*10 (i = 1, 3, and 4) in the other three phen ligands show deviations from planarity ranging from 0.07 to 0.1 Å. Whether these deviations are due to coordination to Mn centers or to crystal packing forces is not known. Nonplanarity of phenanthroline has also been seen—to a smaller extent—in other

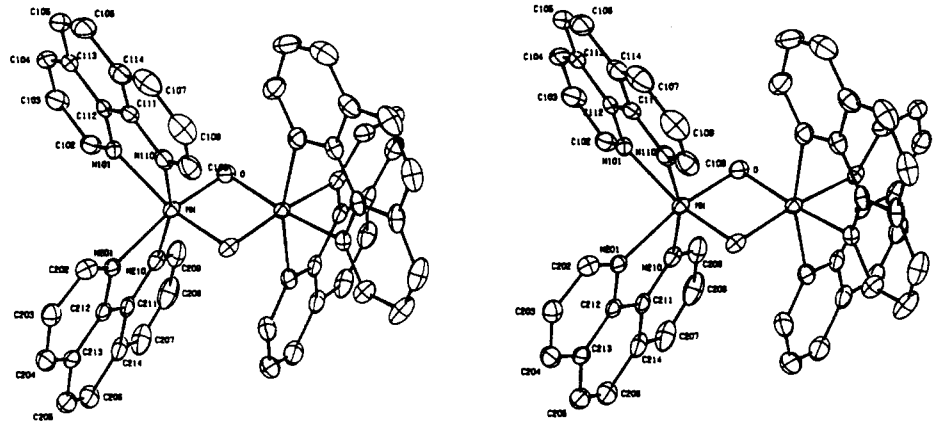

Figure 2. Stereo drawing of a molecule of $[1]^{3+}$ showing the numbering scheme of the complex. Thermal ellipsoids are drawn at 50% probability level.

Table VI. Averaged Distances and Angles of Phenanthroline Rings[a]

Distances, Å

	$[1](ClO_4)_4 \cdot CH_3CN$ 100 K	$[1](PF_6)_3 \cdot CH_3CN$ 100 K	$[1](PF_6)_3 \cdot CH_3CN$ 200 K
N01–N10	2.631 (4)	2.657 (4)	2.652 (8)
N01–C02	1.325 (5)	1.322 (5)	1.325 (7)
C02–C03	1.396 (5)	1.402 (6)	1.387 (7)
C03–C04	1.370 (7)	1.370 (6)	1.367 (9)
C04–C13	1.405 (6)	1.399 (6)	1.396 (8)
C13–C05	1.437 (7)	1.435 (6)	1.435 (9)
C05–C06	1.348 (6)	1.345 (7)	1.339 (9)
C06–C14	1.436 (5)	1.436 (7)	1.438 (9)
C14–C07	1.402 (5)	1.395 (7)	1.394 (9)
C07–C08	1.373 (5)	1.365 (7)	1.360 (9)
C08–C09	1.394 (7)	1.403 (6)	1.398 (7)
C09–N10	1.336 (5)	1.330 (6)	1.324 (7)
N10–C11	1.362 (5)	1.359 (5)	1.358 (7)
C11–C12	1.417 (5)	1.418 (6)	1.413 (7)
C12–N01	1.371 (5)	1.374 (5)	1.375 (8)
C12–C13	1.397 (5)	1.404 (6)	1.396 (7)
C11–C14	1.404 (6)	1.409 (6)	1.404 (8)

Angles, deg

	$[1](ClO_4)_4 \cdot CH_3CN$ 100 K	$[1](PF_6)_3 \cdot CH_3CN$ 100 K	$[1](PF_6)_3 \cdot CH_3CN$ 200 K
C02–N01–C12	117.8 (3)	117.5 (4)	117.1 (5)
C09–N10–C11	119.1 (3)	119.1 (3)	119.2 (5)
N01–C02–C03	122.0 (4)	123.0 (4)	123.2 (5)
N10–C09–C08	121.5 (3)	121.6 (4)	121.9 (5)
C02–C03–C04	120.5 (4)	119.6 (4)	120.0 (5)
C09–C08–C07	120.1 (3)	119.4 (5)	119.1 (6)
C03–C04–C13	119.1 (3)	119.3 (4)	119.0 (5)
C08–C07–C14	119.6 (4)	120.6 (5)	120.9 (6)
C04–C14–C11	116.9 (4)	117.6 (4)	118.0 (5)
C07–C14–C11	117.3 (3)	116.8 (4)	116.7 (5)
N01–C12–C13	123.7 (5)	122.9 (4)	122.9 (4)
N10–C11–C14	122.3 (3)	122.5 (4)	122.3 (5)
C11–C12–C13	120.2 (3)	120.5 (4)	120.6 (5)
C12–C11–C14	121.1 (3)	120.2 (4)	120.3 (5)
C05–C13–C12	117.9 (3)	118.5 (4)	118.3 (5)
C06–C14–C11	117.7 (3)	118.0 (4)	118.1 (4)
C06–C05–C13	121.7 (3)	120.9 (4)	121.4 (6)
C05–C06–C14	121.1 (4)	121.9 (4)	121.3 (6)

[a] Standard deviations were calculated as $\sigma = ((\sum \sigma i^2)/n)^{1/2}$.

structures.[15] The four ClO_4^- anions show no unusual deviation from tetrahedral geometry. The average Cl–O distances range from 1.427 (4) to 1.438 (4) Å.

$[1](PF_6)_3 \cdot CH_3CN$. The following discussion refers to the low-temperature structure (100 K), but the same arguments are valid for the 200 K structure. The complex cation is shown in Figure 2. The site symmetry of the complex is 2, implying that the two

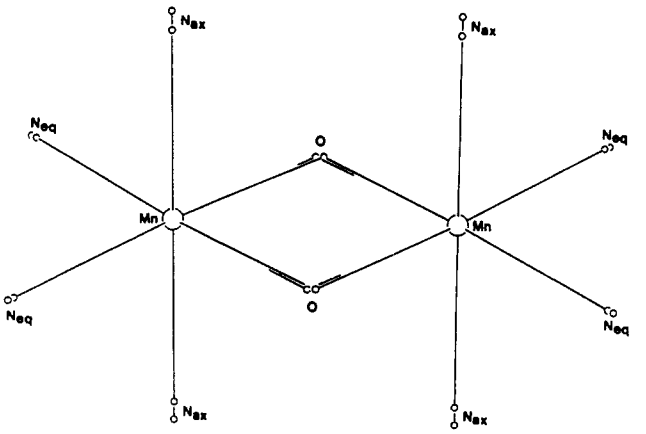

Figure 3. Geometrical model of the disorder in $[1](PF_6)_3 \cdot CH_3CN$.

Mn's are crystallographically equivalent. A priori the equivalence can be explained in three ways: (1) The two Mn's are chemically equivalent, i.e., the seventh Mn d electron is equally shared by the two metal centers (class III;[7] ordered structure). (2) Electron transfer, Mn(III)–Mn(IV) → Mn(IV)–Mn(III), is fast. In the diffraction experiment the two manganese ions appear to be identical (class II;[7] dynamic disorder). (3) The observed structure corresponds to a superposition of a Mn(III)–Mn(IV) and a Mn(IV)–Mn(III) complex (class II or class I;[7] static disorder). Possibility (1) may be distinguished from (2) and (3) on the basis of experimental data. Such a distinction necessitates a careful analysis of the displacement parameters of the molecule as will be discussed below. Possibilities (2) and (3) are not distinguishable from a single X-ray experiment.

Model calculations for metal–ligand bonds in octahedral metal complexes based on vibrational spectroscopy have shown[16] that intramolecular motion is significant and different for the metal (M) and the ligand (L). This is reflected in different mean-square displacements along the M–L bond vector ($U_{intra}(L,z)$, $U_{intra}(M,z)$):

$$\Delta U_{intra}(ML,z) = U_{intra}(L,z) - U_{intra}(M,z) > 0$$

Calculated values ΔU_{intra} are generally in the range (10–30) × 10^{-4} Å^2 and agree well with values based on observed displacement parameters (temperature factors, U_{obsd}):

$$\Delta U_{obsd}(ML,z) = U_{obsd}(L,z) - U_{obsd}(M,z) \approx \Delta U_{intra}(ML,z)$$

Sometimes, however, ΔU_{obsd} values are significantly larger. In such cases the molecules usually show dynamic or static distortion with large amplitude. The effect of distortion (ΔU_{dist}) must be included in the difference displacement parameters, i.e.

$$\Delta U_{obsd}(ML,z) \approx \Delta U_{intra}(ML,z) + \Delta U_{dist}(ML,z)$$

The additional contribution ΔU_{dist} may be 1 or 2 orders of

(15) Veal, J. T.; Hatfield, W. E.; Hodgson, D. J. *Acta Crystallogr., Sect. A: Cryst. Phys., Diffr., Theor. Gen. Crystallogr.* **1976**, *A32*, 239.

(16) Chandrasekhar, K.; Bürgi, H.-B. *Acta Crystallogr., Sect. B: Struct. Sci.* **1984**, *B40*, 387.

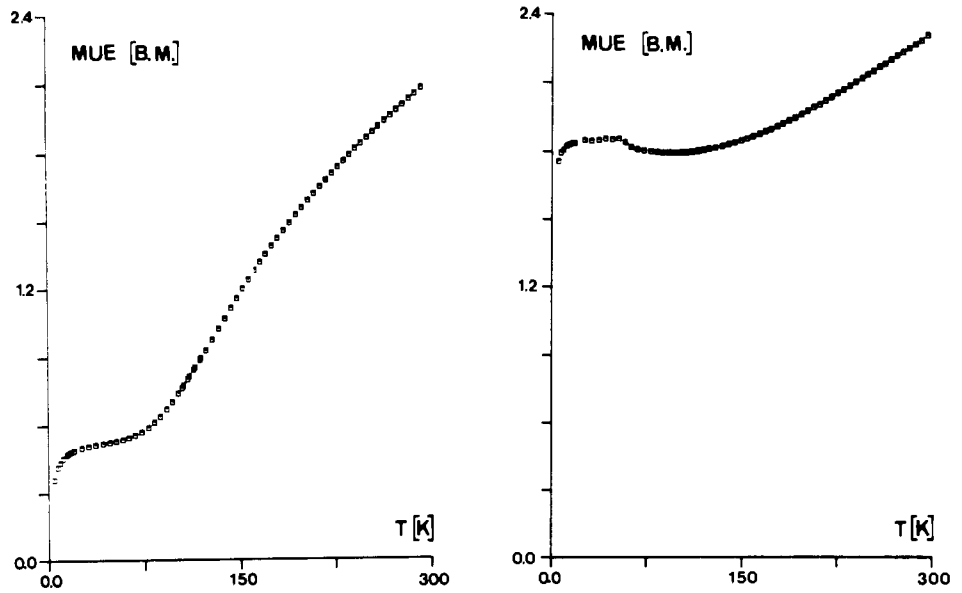

Figure 4. Temperature dependence of the magnetic moment of $[1](ClO_4)_4 \cdot CH_3CN$ (left) and $[1](PF_6)_3 \cdot CH_3CN$ (right).

magnitude larger than the values for $\Delta U_{intra}(ML,z)$.[16-18]

Superficial inspection of $\Delta U_{obsd}(ML,z)$ values (Table V) for the mixed-valence complex $[1]^{3+}$ and comparison to those of $[1]^{4+}$ indicate the possibility of static or dynamic disorder of $[1]^{3+}$. A detailed examination was carried out in two steps: (1) A geometrical model for disorder was developed on the basis of the bond lengths for compound $[2](ClO_4)_3 \cdot 3H_2O$,[5] and its consequences on ΔU_{obsd} were calculated. (2) The difference mean-square amplitudes $\Delta U_{obsd}(ML)$ observed for $[1]^{3+}$ were evaluated and compared with the values derived from the geometrical model.

If the Mn–N and Mn–O distances of the two different metal centers in $[2]^{3+}$ are averaged, assuming $2/m$ symmetry of the cation, the calculated coordination geometry of this "Mn(III)–Mn(IV) ion" corresponds to within estimated standard deviations to the observed coordination geometry of $[1]^{3+}$ (Table V).[19] The following model for a disordered structure of $[1]^{3+}$ is therefore postulated: The observed mean geometry results from the superposition of Mn(III) and Mn(IV) ions: $^1/_2$[Mn(III)–Mn(IV)] + $^1/_2$[Mn(IV)–Mn(III)] with Mn–O and Mn–N distances as observed in $[1]^{3+}$ (Figure 3). In this model, there are two half N atoms separated by $\Delta d(Mn–N) \approx 0.191$ Å. During structure refinement this was simulated by a single nitrogen atom in intermediate position with an enlarged mean-square displacement to account for the disorder. An estimate of the enlargement $\Delta U_{dist}(MnN,z)$ may be obtained as follows: As a first approximation, it is assumed that the contribution ΔU_{dist} to ΔU_{obsd} equals the second moment of two δ functions positioned at $\pm\Delta d(Mn–N)/2$ (with weight $p = ^1/_2$).

$$\Delta U_{dist} = \sum_i p_i(\Delta d/2)^2 = 2^1/_2(\Delta d/2)^2 = \Delta d^2/4$$

The value for $\Delta U_{intra}(MnN,z)$ is taken from $[1]^{4+}$ which shows no distortion. Indeed, the observed values (Table V)[20] for this complex are in the normal range[16,17] $\sim 30 \times 10^{-4}$ Å^2.

The estimated values $\Delta U_{intra} + \Delta U_{dist}$ which are large for the axial N's and comparably small for the equatorial N's and O's may now be compared to the observed values. The average observed values for the low-temperature structure of $[1]^{3+}$ coincide very well with the estimated values (Table VII). The excellent agreement between the model and the observations shows that $[1]^{3+}$ has a disordered structure. The possibility that the mixed-valence cation is ordered can now be excluded with certainty. However, it is not possible to distinguish between dynamic and statistical static disorder; in both cases the dependence of the displacement parameters of the ligands on bond length differences is of the same form.

Table VII. ΔU(MnL) Estimated from the Geometrical Model and Observed from Diffraction Data for $[1](PF_6)_3 \cdot CH_3CN$

Mn–L	Δd(MnL), Å	$(\Delta d/2)^2$, Å^2	$\Delta U_{intra} + \Delta U_{dist}$, Å^2	ΔU_{obsd}(MnL), Å^2
$Mn–N_{eq}$	0.057	0.0008	0.0038	0.0014 (25)
$Mn–N_{ax}$	0.195	0.0095	0.0125	0.0135 (24)
Mn–O	0.071	0.0013	0.0043	0.0037 (21)

The four-membered ring of $[1]^{3+}$ is not planar; the bridging oxygen atoms are 0.03 Å above the least-squares plane. Although the Mn–O bond length in the mixed-valence compound are longer than in the oxidized Mn(IV)–Mn(IV) complex, the Mn(III)–Mn(IV) distance (2.700 Å) is shorter. These data indicate a somewhat stronger attractive force (one-electron more!) between the metal atoms in the Mn(III)–Mn(IV) cation than in the Mn(IV)–Mn(IV) complex. The Mn–Mn and the Mn–O distances found in an EXAFS study[2] agree very well with the distances found in the present single-crystal structure determination.

Again, as in $[1]^{4+}$, two phenanthroline ligands complete the coordination around the manganese atom. The averaged values of the bond lengths and angles of the ligands, assuming $2/m$ symmetry, are listed in Table VI; a full list is given as supplementary material. As in $[1](ClO_4)_4 \cdot CH_3CN$ the phenanthrolines are not planar; one ligand shows only small deviations from planarity, whereas the other one is much less planar; the largest deviation is 0.11 Å, the positional standard deviations of the atoms defining the plane are ~0.06 Å.

PF_6^- in general position and one of the disordered anions ([PF_6(2)]) are almost perfectly octahedral with average P–F bond lengths of 1.602 (4) and 1.593 (3) Å, respectively; the anion [PF_6(3)] is somewhat distorted. The P–F bond lengths are in the range of 1.574–1.604 Å with an average of 1.584 (30) Å; the average angles F–P–F are 169.7 (3)° and 90 (3)°. The standard deviations of the bond lengths and angles of [PF_6(3)], [CH_3CN(2)], and [CH_3CN(3)] are very large, reflecting the low significance of the derived geometrical information.

Magnetic Data. The temperature dependence of the effective magnetic moments of $[1](PF_6)_3 \cdot CH_3CN$ and $[1](ClO_4)_4 \cdot CH_3CN$ is shown in Figure 4. It is found that μ_{eff} of $[1](PF_6)_3 \cdot CH_3CN$ decreases from 2.3 μ_B at room temperature to ~1.6 μ_B at ~3 K. For $[1](ClO_4)_4 \cdot CH_3CN$ the decrease of μ_{eff} from ~2.1 to ~0.6

(17) Ammeter, J. H.; Bürgi, H.-B.; Gamp, E.; Meyer-Sandrin, V.; Jensen, W. P. *Inorg. Chem.* **1979**, *18*, 733.
(18) Stebler, M. Dissertation, Universität Bern, Bern, 1985.
(19) Although this coincidence is suggestive, it does not necessarily exclude an ordered structure for $[1]^{3+}$ (chemically equivalent manganese centers).
(20) The difference displacement parameters of $[2]^{3+}$ are somewhat erratic (some are very large, some are negative), but they are of the same order as their standard deviations. This reflects the limited quality of the crystal structure determination.[5]

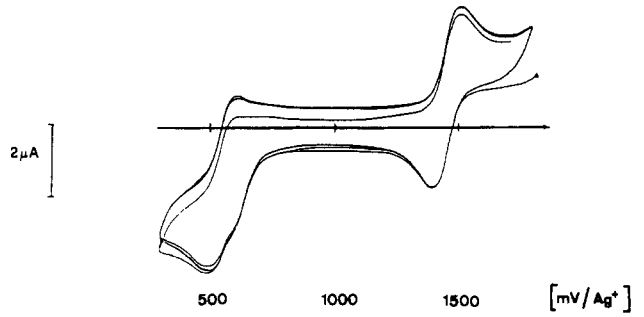

Figure 5. Cyclic voltammogram of $[1](ClO_4)_4 \cdot CH_3CN$ in 0.1 M $[(C_4H_9)_4N]ClO_4/CH_3CN$ (Pt electrodes; scan rate = 100 mV s^{-1}).

μ_B is an almost linear function of temperature in the range 80–300 K. Paramagnetic impurities seem to be responsible for the behavior of μ_{eff} below ~75 K in both compounds. Alternatively, intermolecular interactions may be invoked to explain μ_{eff} below 75 K. The latter possibility would seem less likely in view of the bulky hydrocarbon ligands encapsulating the metal ions and effectively shielding them from other metal ions. Diagrams of observed and calculated values of $\chi(T)$ are given as supplementary material.

Interpretation of the magnetic data based on an isotropic Heisenberg operator ($H_{ex} = -2JS_1S_2$; S_1 and S_2 = spin on Mn1 and Mn2, respectively) yields the following values for the exchange coupling constants J and the g factors: −148 (12) cm^{-1} and 1.999 for $[1](PF_6)_3 \cdot CH_3CN$ and −144 (7) cm^{-1} and 1.96 for $[1](ClO_4)_4 \cdot CH_3CN$. J values for $[1]^{3+}$ and $[1]^{4+}$ are nearly equal as might be expected from the small structural difference in the MnO_2Mn fragment. The values[4] of −134 (5) cm^{-1} for $[1](ClO_4)_3 \cdot CH_3COOH$ and −150 (7) cm^{-1} for $[2](ClO_4)_3 \cdot 2H_2O$ (g was kept at 2.003 in both cases) are in good agreement with the result for the PF_6^- salt. The numbers indicate that there is no significant difference in magnetic behavior due to the different ligands.

Optical Spectroscopy. The UV–vis spectrum of $[1](ClO_4)_4 \cdot CH_3CN$ shows two weak shoulders at ~425 and ~510 nm (possibly d–d transitions) on the side of a very strong absorption at ~400 nm. The spectrum of $[1](PF_6)_3 \cdot CH_3CN$ shows two shoulders at 523 (ϵ = 580) and 550 nm (ϵ = 460 M^{-1} cm^{-1}, possibly d–d transitions). Another absorption is observed at 680 nm (ϵ = 550 M^{-1} cm^{-1}) with a broad shoulder at ~800 nm. The spectrum is very similar to that of $[2](ClO_4)_3 \cdot 3H_2O$.[3] Several interpretations of the absorption band at 680 and 800 nm have been given in the literature.[3,21,22]

The intensity of the absorption at ~800 nm increases with decreasing temperature; that of the absorption at 680 nm is temperature independent.[23] If the former absorption is tentatively assigned to some kind of intervalence transition, then the classical barrier for thermal hopping of the odd d electron is estimated to be at ~3000 cm^{-1}. This barrier may also be estimated from the structural data on $[2](ClO_4)_3 \cdot 3H_2O$ as $\Delta E = 4k(MnN_{ax})\{\Delta d(MnN_{ax})/2\}^2/2 + 4k(MnN_{eq})\{\Delta d(MnN_{eq})/2\}^2/2 + 4k(MnO)\{\Delta d(MnO)/2\}^2/2$. If all three force constants are assumed to equal ~2 mdyn/Å, the estimated value of ΔE is ~2400 cm^{-1}.

Cyclic Voltammetry. A solution of $[1]^{3+}$ shows two waves in the cyclic voltammetry, one at 340 mV and the other at 1280 mV vs. NHE. Both signals correspond to one-electron processes according to $[1]^{4+} + e \rightleftharpoons [1]^{3+}$, 1280 mV, and $[1]^{3+} + e \rightleftharpoons [1]^{2+}$, 340 mV. From the difference of the two reduction potentials a value of 10^{16} is inferred for the comproportionation constant, in agreement with earlier studies.[3] We have carried out the same experiment with a solution of $[1]^{4+}$. The wave corresponding to the back oxidation $[1]^{2+}$ to $[1]^{3+}$ is very weak and depends on the scan rate. We attribute this apparently irreversible redox reaction, not observed for the wave at 1280 mV, which shows Nernstian behavior, to a fast comproportionation reaction depleting the immediate neighborhood of the electrode of the reduced species $[1]^{2+}$. Moreover, from the general feature of this redox step (Figure 5) partial dissociation of the reduced dimer cannot be excluded as an additional complication.

Acknowledgment. We thank Dr. P. Baltzer, University of Zürich, for magnetic measurements, Dr. A. Hauser, University of Berne, for optical measurements, and Dr. A. Gutierrez for his help in preparing the manuscript.

Registry No. $[1](PF_6)_3 \cdot CH_3CN$, 105121-91-3; $[1](ClO_4)_4 \cdot CH_3CN$, 105121-92-4.

Supplementary Material Available: Listings of atomic coordinates, anisotropic displacement parameters, hydrogen positions, bond lengths and angles, and observed and calculated magnetic data for $[1](ClO_4)_4 \cdot CH_3CN$ at 100 K and $[1](PF_6)_3 \cdot CH_3CN$ at 100 and 200 K and Figure S1, showing the observed and calculated temperature dependence of the magnetic susceptibility of $[1](ClO_4)_4 \cdot CH_3CN$ and $[1](PF_6)_3 \cdot CH_3CN$ (14 pages); listings of observed and calculated structure factors for $[1](ClO_4)_4 \cdot CH_3CN$ at 100 K and $[1](PF_6)_3 \cdot CH_3CN$ at 100 and 200 K (68 pages). Ordering information is given on any current masthead page.

(21) Dingle, R. *Acta Chem. Scand.* **1966**, *20*, 33.
(22) Davis, T. S.; Fackler, J. P.; Weeks, M. J. *Inorg. Chem.* **1968**, *7*, 1994.
(23) The temperature dependence of the spectrum is still under investigation. Raselli, A.; Güdel, H. U., unpublished results and ref 18.